LETTER

Collisionless pitch-angle scattering of runaway electrons

IOP Publishing | International Atomic Energy Agency Nuclear Fusion

Nucl. Fusion **56** (2016) 064002 (7pp) doi:10.1088/0029-5515/56/6/064002

Letter

Collisionless pitch-angle scattering of runaway electrons

Jian Liu[1,2], Yulei Wang[1,2] and Hong Qin[1,3]

[1] School of Nuclear Science and Technology and Department of Modern Physics, University of Science and Technology of China, Hefei, Anhui 230026, People's Republic of China
[2] Key Laboratory of Geospace Environment, CAS, Hefei, Anhui 230026, People's Republic of China
[3] Plasma Physics Laboratory, Princeton University, Princeton, NJ 08543, USA

E-mail: hongqin@ustc.edu.cn

Received 26 December 2015, revised 4 April 2016
Accepted for publication 8 April 2016
Published 11 May 2016

Abstract

It is discovered that the tokamak field geometry generates a toroidicity induced broadening of the pitch-angle distribution of runaway electrons. This collisionless pitch-angle scattering is much stronger than the collisional scattering and invalidates the gyro-center model for runaway electrons. As a result, the energy limit of runaway electrons is found to be larger than the prediction of the gyro-center model and to depend heavily on the background magnetic field.

Keywords: runaway electron, neoclassical scattering, pitch-angle scattering, volume-preserving algorithm, energy limit, gyro-center model, toroidal geometry

(Some figures may appear in colour only in the online journal)

Runaway electrons in a tokamak are energetic particles accelerated by the electric field. They cannot be braked by collisional drag [1]. A large number of runaway electrons are produced in tokamaks during fast shutdowns, disruptions [2–15], or aggressive current drive [16]. It has been experimentally observed that the runaway electron energy can reach tens of MeVs or higher with the volt-seconds available in disruptions at various tokamaks [17–24]. The massive energy carried by runaway beams poses great danger to plasma-facing components [25–28]. Understanding the physics of runaway electrons in toroidal field configurations is thus critical. The dynamics of runaway electrons involves different timescales spanning 11 orders of magnitude, which brings difficulties to both analytical and numerical studies. A gyro-center model is often applied to tackle the multiscale problem by averaging out the fast gyro-motion and has produced fruitful results [29–37]. According to the gyro-center model, the magnetic moment of runaway electrons is an adiabatic invariant, and the parallel momentum increases due to the work by the loop electric field. There is no channel of momentum transfer from the parallel to the perpendicular direction, except for collision with background plasmas. In general, the collisional effect is rather weak for charged particles with high velocities [33]. For a typical runaway electron, the collision time is $\tau_{\rm col} \sim 0.5$ s, which is much longer than the gyro-period $T_{\rm ce}$ ($\sim 10^{-10}$ s) and the transit period $T_{\rm tr}$ ($\sim 10^{-8}$ s). When the collisional effect can be neglected, the perpendicular momentum will monotonically decrease due to the synchrotron radiation of the gyro-motion [33], and parallel momentum will monotonically increase to its maximum limit until the electric field acceleration is finally balanced by the radiation dissipation. The pitch-angle scattering due to collisions will transfer a small amount of energy from the parallel direction to the perpendicular direction. This small collisional effect keeps the runaway electrons energetic in the perpendicular direction, but does not modify the energy limit in the parallel direction by much. The gyro-center model predicts that the energy limit of runaway electrons does not depend on collisions or the magnitude of the background magnetic field [29].

Contrary to the common wisdom, our analysis shows that the gyro-center model is not valid for runaway electrons. In general, for the gyro-center model to be valid, a necessary condition is that the variation of magnetic field experienced by a charged particle in one gyro-period is very small, i.e.

$|\Delta \mathbf{B}/\mathbf{B}|_T \ll 1$, where $T = 2\pi\gamma m_{rest}/QB$ is the gyro-period, Q denotes the charge of particle, m_{rest} is the rest mass, and γ is the Lorentz factor. This variation of magnetic field is due to both the perpendicular gyro-motion and the parallel motion along the magnetic field line. Therefore, for the gyro-center model to be valid, it is required that $\rho/R \ll 1$, which is the statement that the variation of magnetic field due to perpendicular gyro-motion is very small. It is also required that the variation of magnetic field that the charged particle experiences while travelling along the magnetic field line in one gyro-period be very small, i.e. $Tv_\parallel/R \ll 1$. This second necessary condition has been clearly stated in the standard references on gyro-center dynamics, e.g. Littlejohn's papers [38, 39] and Northrop's book [40]. Here, ρ is the gyro-radius, $v_\parallel$ is the parallel velocity, and R is the scale-length of magnetic field, i.e., the major radius, in tokamaks. For typical runaway electrons in tokamaks, the condition $\rho/R \ll 1$ satisfies, but $Tv_\parallel/R \ll 1$ does not. The large parallel velocity and the increased relativistic mass of runaway electrons result in a significant change of position in the toroidal direction in one gyro-period and the breakdown of basic gyro-center assumptions. In fact, the magnetic moment μ is no longer an adiabatic invariant. Similar non-conservation of μ has been observed in the presence of magnetic turbulence with wavelength comparable to the gyro-radius [41, 42]. As the lowest order approximation for the invariant magnetic moment, μ is not conserved in many circumstances. The non-adiabatic jumps of magnetic moment corrected to higher-order terms of asymptotic series have been discussed in [43, 44], where the breakdown of adiabatic dynamics of charged particles in regions of weak field are investigated both analytically and numerically.

In this letter, we abandon the gyro-center model and study the multi-timescale runaway dynamics by numerically solving the dynamical equations of runaway electrons directly in the six-dimensional phase space. Long-term simulation results confirm that the gyro-center model is indeed invalid, see figure 2. More than one hundred billion time steps are required in the simulation. To eliminate the coherent accumulation of numerical errors from each time step, which is usually a show-stopper for long-term simulations, we utilize the newly developed volume-preserving algorithm (VPA) for relativistic particles [45]. The VPA can guarantee long-term accuracy by preserving the phase-space volume of the original physical system. Its long-term conservativeness and stability have been verified.

Taking the advantage of the VPA method, we discovered that there exists a collisionless pitch-angle scattering mechanism, which transfers momentum of runaway electrons between the parallel and perpendicular directions. It arises from the full orbit dynamics in the toroidal geometry of a tokamak via a toroidicity induced broadening of the pitch angle distribution of runaway electrons. The collisionless pitch-angle scattering process is about a million times faster than the collisional pitch-angle scattering, resulting in a rapid transfer of the parallel momentum, gained from the loop electric field, to the perpendicular direction. As an important result, the simulation study indicates a new energy limit for runaway electrons, which is higher than the result from the gyro-center model and varies with the magnitude of the background magnetic field. This unexpected collisionless pitch-angle scattering effect for runaway electrons and its important consequence are the subjects of this letter.

First, we introduce the physical model. When focusing on the long-term dynamics of runaway electrons in a tokamak, we take into account the background magnetic field, the loop electric field, and the electromagnetic radiation. The dynamical equations of runaway electrons are

$$\frac{d\mathbf{x}}{dt} = \mathbf{v}, \tag{1}$$

$$\frac{d\mathbf{p}}{dt} = -e(\mathbf{E} + \mathbf{v} \times \mathbf{B}) + \mathbf{F}_R, \tag{2}$$

$$\mathbf{p} = \gamma m_0 \mathbf{v}, \tag{3}$$

where $\mathbf{x}$, $\mathbf{v}$, $\mathbf{p}$ denote the position, velocity and mechanical momentum of a runaway electron, e denotes the unit charge, m_0 is the rest mass of electron, $\mathbf{E}$ and $\mathbf{B}$ are the electric and magnetic field, and the Lorentz factor γ is defined as

$$\gamma = \sqrt{1 + \frac{p^2}{m_0^2 c^2}} = \frac{1}{\sqrt{1 - (v/c)^2}}. \tag{4}$$

The effective electromagnetic radiation drag force $\mathbf{F}_R$ is

$$\mathbf{F}_R = -P_R \frac{\mathbf{v}}{v^2}, \tag{5}$$

where P_R is the radiation power determined by [46]

$$P_R = \frac{q_e^2}{6\pi\epsilon_0 c}\gamma^6 \left[\left(\frac{\mathbf{a}}{c}\right)^2 - \left(\frac{\mathbf{v}}{c} \times \frac{\mathbf{a}}{c}\right)^2\right]. \tag{6}$$

Here, ϵ_0 is the permittivity of a vacuum, c is the speed of light in vacuum, and $\mathbf{a} = d\mathbf{v}/dt$ denotes the acceleration.

In order to solve equations (1) and (2) numerically, we have to meet the challenge brought by the multi-scale nature of the problem. Restricted by the minimal timescale, more than 10^{11} time-steps are required to simulate a complete runaway dynamics. Traditional algorithms, such as the 4th order Runge–Kutta method, are not qualified for this long-term simulation, because the coherent accumulation of numerical error over many time-steps leads to incorrect long-term simulation results. To overcome this difficulty, geometric algorithms which can bound the global numerical error for all time-steps should be adopted [45, 47–51]. The newly developed relativistic VPA [45] with radiation drag is utilized in the present study to guarantee the long-term numerical accuracy.

When the synchrotron radiation is included in the model for runaway electrons, the familiar canonical angular momentum is no longer an invariant of the dynamics. This is because the radiation reaction force is a dissipative effect and no rigorous treatment has been discovered to include the radiation reaction force in the Lagrangian. If such a Lagrangian can be found in the future, then it is possible to define a new invariant canonical angular momentum. However, in one transit period, the momentum loss due to radiation is in general small, and one can ask whether the theoretical model and

numerical algorithms adopted conserve the familiar canonical angular momentum when the radiation reaction is ignorable. This study has been carried out in [45], where the integrable dynamics of a runaway electron without radiation reaction is simulated using the same theoretical model and relativistic VPA adopted in the present study. Zhang *et al* [45] show that the VPA conserves canonical toroidal angular momentum. After more than 10^8 time steps, the relative numerical error of the canonical toroidal angular momentum is still bounded in a very small value.

Because the tokamak equilibrium magnetic field is symmetric in the toroidal direction, it is convenient to use the cylindrical coordinate to express the background magnetic field and inductive electric field as

$$\mathbf{B} = -\frac{B_0 R_0}{R}\mathbf{e}_\xi - \frac{B_0\sqrt{(R-R_0)^2+z^2}}{qR}\mathbf{e}_\theta\,, \tag{7}$$

$$\mathbf{E} = E_l\frac{R_0}{R}\mathbf{e}_\xi\,, \tag{8}$$

where $R=\sqrt{x^2+y^2}$, ξ, and z are radial distance, azimuth, and height of the cylindrical coordinate system respectively, $\mathbf{e}_\xi$ and $\mathbf{e}_\theta$ are the unit vectors along toroidal and poloidal directions, and q denotes safety factor. The z-component of magnetic field B_z is in the negative z-direction when $R > R_0$, and positive z-direction when $R < R_0$. This magnetic configuration is the geometric origin of the collisionless pitch-angle scattering. Without loss of generality, we use the parameters of a typical Tokamak. The major radius is $R_0 = 1.7$ m, the safety factor is $q = 2$, the central magnetic field is $B_0 = 3$ T, and the loop electric field is $E_l = 0.2$ V m^{-1}. The initial parallel and perpendicular momentum of a typical runaway electron are set to be $p_{\|0} = 5\ \mathrm{m_0c}$ and $p_{\perp 0} = 1\ \mathrm{m_0c}$, and the initial position is $R = 1.8$ m and $\xi = z = 0$. The time-step of simulation is set to $\Delta t = 1.9\times10^{-12}$ s, which is about 1% of the gyro-period.

Figure 1 depicts the snapshots of runaway orbit projected in the poloidal plane at different times. It shows evident outward neoclassical drift in the poloidal plane similar to Guan *et al*'s result [33]. On the other hand, there exit small-scale ripple structures during each transit period, which cannot be recovered by the gyro-center model. These ripples correspond to the toroidal elongation of runaway orbits due to energy increasing. There are 30 to 40 ripples in snapshots at 2 s, which indicates the runaway electron undergoes 30 to 40 gyro-periods during one transit period.

To verify that the condition for gyro-center approximation is not satisfied for runaway electrons in tokamaks, we record the change ratio of the magnetic field $\Lambda_{\mathrm{B}}(t)$ that one runaway electron samples during one gyro-period at different time t, see figure 2. The change ratio is defined as

$$\Lambda_{\mathrm{B}}(t) = \frac{|\mathbf{B}(t+T_{\mathrm{ce}}) - \mathbf{B}(t)|}{|\mathbf{B}(t)|}\,, \tag{9}$$

where $T_{\mathrm{ce}} = 2\pi\gamma \mathrm{m_0}/eB$ is the gyro-period. For the gyro-center approximation to be valid, the variation of the magnetic field a particle samples during one gyro-period should be small.

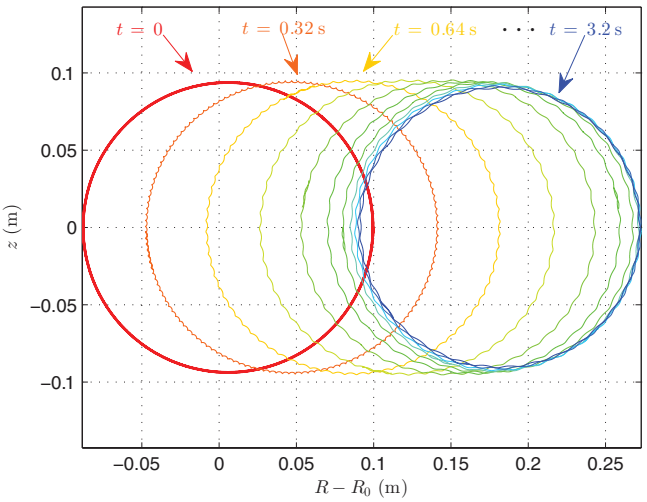

Figure 1. Snapshots of runaway orbit projected in the poloidal plane at different time. Parameters of the electromagnetic field are $R_0 = 1.7$ m, $a = 0.4$ m, $q = 2$, $B_0 = 3$ T and $E_l = 0.2$ V m^{-1}. Initial momentum of the runaway electron is $p_{\|0} = 5\ \mathrm{m_0c}$ and $p_{\perp 0} = 1\ \mathrm{m_0c}$. Initial position is $R = 1.8$ m and $\xi = z = 0$. In addition to the neoclassical radial drift, ripple structures in the transit orbit are observed.

However, simulation results show that the change ratio Λ_{B} increases monotonically with the runaway energy. Its value increases to 10% after 0.4 s and exceeds 30% after 1.7 s, which can no longer be taken as a small value. This is mainly because the velocity of runaway electron approaches the speed of light, and the gyro-period T_{ce} is proportional to the Lorentz factor γ. The runaway electron travels a long distance along the toroidal direction during each gyro-period, which leads to a significant rotation of magnetic field faced by the particle and thus a large value of Λ_{B}. Even though 20% or 30% is a modest number, a theorist may still argue that it is a small number from a purely theoretical point of view. We emphasize that what really matters here is whether the magnetic moment can hold constant for a sufficiently long time, i.e. the lifetime of the runaway electrons. Our full orbit simulations show that the 21% variation of the magnetic field in one gyro-period is able to break the invariant of the magnetic moment in one or several gyro-periods, and invalidates the gyro-center model. Unlike the randomly uncorrelated cases in [43, 44], the collisionless scattering of runaway dynamics in the tokamak field is correlated during each gyro-period and exhibits a long-term accumulation effect, which results in the breakdown of gyro-center condition. Therefore, full orbit calculations must be used to understand the long-term phase space dynamics of runaway electrons.

The momentum evolution of runaway electrons is plotted in figure 3. A band structure appears in the time history of both the perpendicular and the parallel momentum. The band in figure 3(*a*) is narrow, and can only be identified in the zoomed in window. The band structures are due to fast oscillation of the components of the momentum. Because the absolute value of the parallel momentum is large, its oscillation is less prominent. When zooming in, the momentum vector rotates during every gyro-period—see figure 4. The overall increase of the

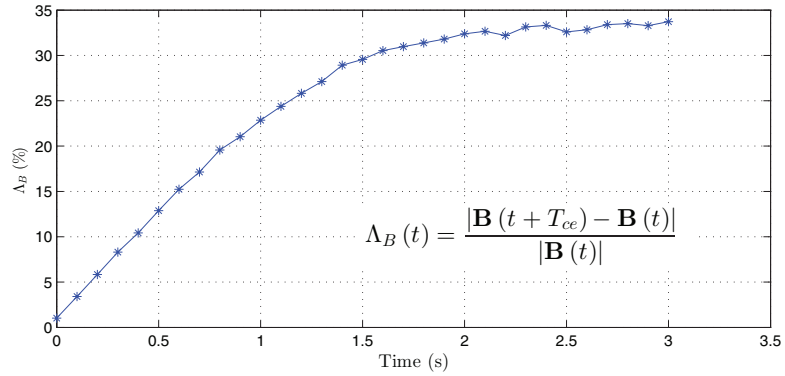

Figure 2. Change ratio of background magnetic field Λ_B during one gyro-period at different times of a runaway dynamics. The significant increase of Λ_B mainly corresponds to the accumulated change of direction of the magnetic field in one gyro-period.

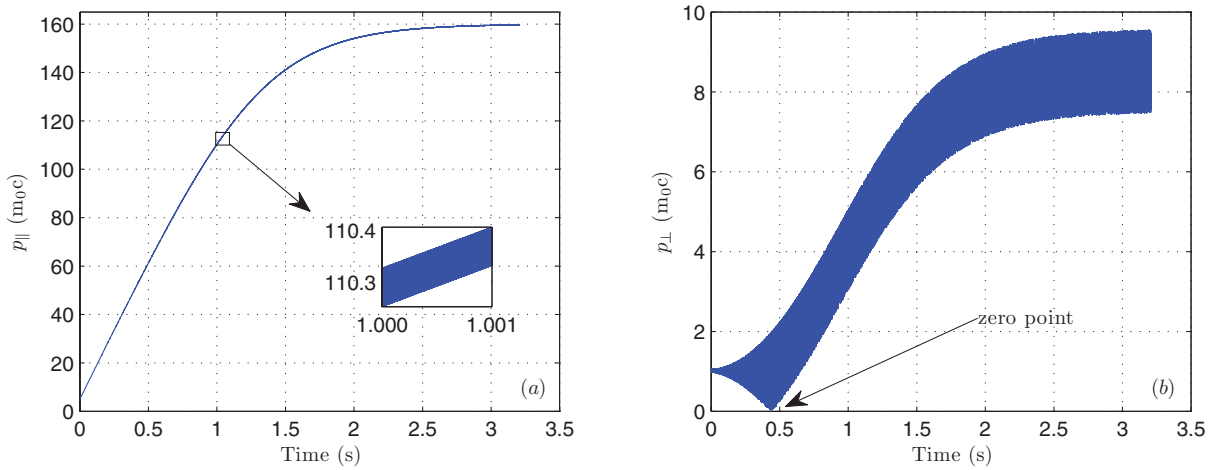

Figure 3. Evolution of (*a*) parallel momentum and (*b*) perpendicular momentum of a runaway electron. The zoomed-in window for the parallel momentum curve between 1 s and 1.001 s shows an oscillation band similar to that for the perpendicular momentum. Initial position of the electron is at $R = 1.8$ m, $\xi = z = 0$, and its initial momentum is $p_{\|} = 5\ m_0c$ and $p_{\perp} = m_0c$. The center magnetic field is $B_0 = 3$ T and the loop electric field is $E_l = 0.2$ V m^{-1}.

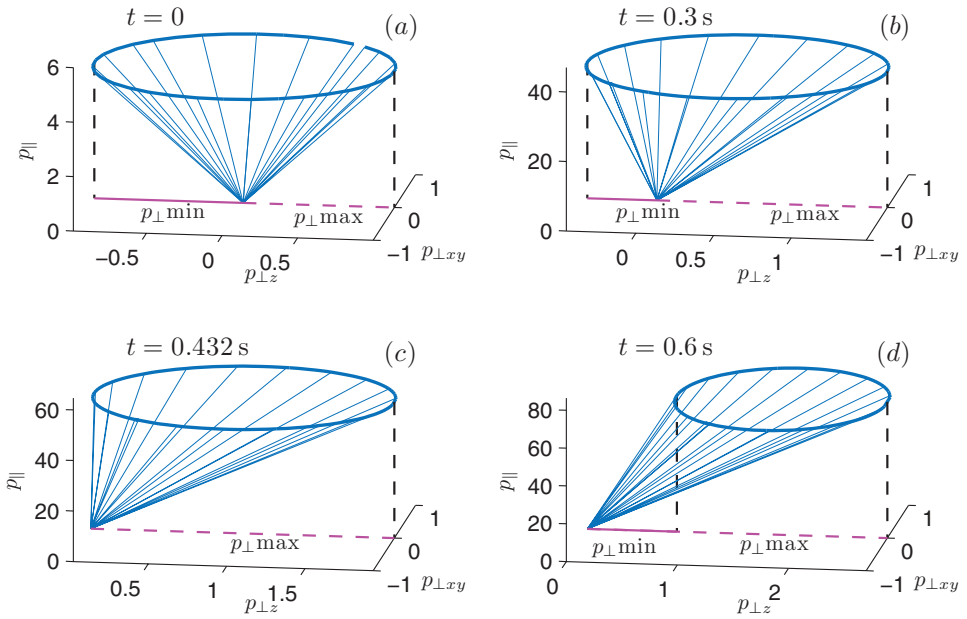

Figure 4. Motion of the momentum vector during one gyro-period at different time. The maximal and minimal perpendicular momenta, $p_{\perp\max}$ and $p_{\perp\min}$, during each gyro-period are marked by the dashed line.

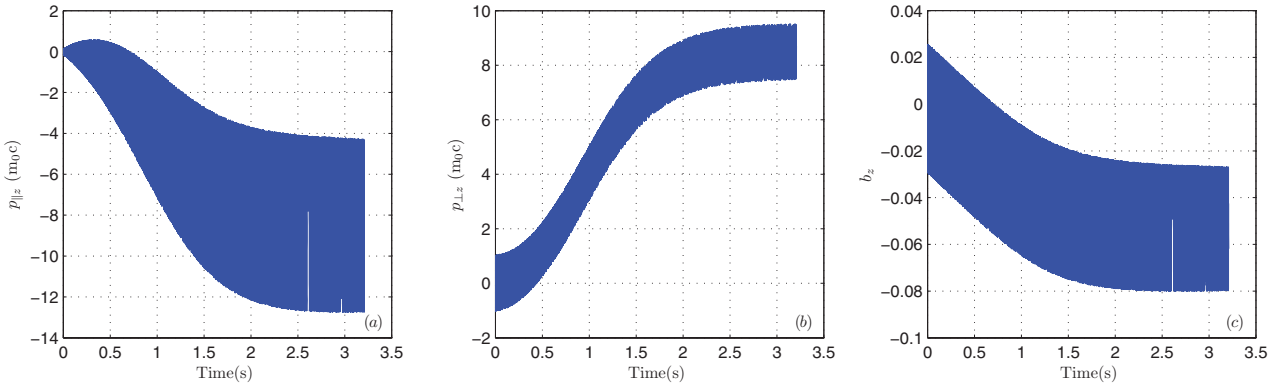

Figure 5. Evolution of (*a*) *z*-component of parallel momentum $p_{\|z}$, (*b*) *z*-component of perpendicular momentum $p_{\perp z}$, and (*c*) *z*-component of unit vector along the magnetic field b_z.

parallel momentum is similar to the results from the gyro-center model [31, 33], but the evolution of the perpendicular momentum is very different. The perpendicular momentum grows with rapid oscillations, even in the absence of collisions, until approaching a maximum after about 2.5 s. Because the parallel momentum is relatively large, its oscillation is less prominent. The oscillation is an effective scattering process transferring the parallel momentum to the perpendicular direction and altering the pitch-angle. As explained later, this effective pitch-angle scattering roots in the geometric configuration of the field. It is thus a collisionless pitch-angle scattering effect. The evolution of the perpendicular momentum exhibits four stages: (a) a rapid oscillation is developed initially; (b) then its absolute value reaches the zero point; (c) it grows quickly after passing the zero point, and (d) it saturates. At the saturation, though the pitch-angle still varies quickly due to the collisionless scattering, the average perpendicular momentum does not change. The timescale of collisionless pitch-angle scattering is 5×10^{-7} s, which is about 10^6 times faster than the collisional scattering, and much more momentum can be transferred to the perpendicular direction through the collisionless scattering than the collisional effect as calculated in [33].

The seemingly complex evolution curves of the perpendicular momentum are dominated by the collisionless scattering, which can be analyzed by looking at the variation of the momentum vector. We choose the parallel momentum $p_\|$, the *z*-component of the perpendicular momentum $p_{\perp z}$, and the projection of perpendicular momentum in the *x*–*y* plane $p_{\perp xy}$ as the three coordinates for the momentum. They satisfy $p_{\perp xy}^2 + p_{\perp z}^2 + p_\|^2 = p^2$. In figure 4, snapshots of the momentum vector within one gyro-period at different moments are plotted in the momentum space. During each gyro-period, the tip of the momentum vector moves approximately along a circular orbit. The minimal and maximal value of $p_{\perp z}$ are marked within each gyro-period. The circular orbit is first elongated while the center of circle shifts to $p_{\perp z}$ direction in the perpendicular plane. The elongation of the orbit corresponds to the growth of the oscillation amplitude. At $t = 0.432$ s, the orbit touches the $p_{\perp z} = 0$ plane, and the zero point of perpendicular momentum appears. Afterwards, the elongated orbit keeps shifting towards the larger $p_{\perp z}$ direction until approaching a steady state. It is evident that the variation of $p_\perp$ is mainly due to the *z*-component $p_{\perp z}$.

Figure 5 shows the evolution of the *z*-component of the parallel momentum $p_{\|z}$, the *z*-component of the perpendicular momentum $p_{\perp z}$, and the *z*-component of the unit vector along the magnetic field $b_z = \mathbf{b} \cdot \mathbf{z} = \mathbf{B} \cdot \mathbf{z}/B$. We find that $p_{\perp z}$ increases, oscillates, and saturates around $9\ m_0c$. The oscillation amplitude of $p_{\|z}$ increases with the absolute value of $p_\|$. Meanwhile, the evolution of $p_{\|z}$ has the same trend as b_z, which indicates that the collisionless scattering is closely related to the direction of the local magnetic field. Due to neoclassical drift [33, 34], the transit orbits of runaway electrons drift outwards from the magnetic axis. As a result, runaway electrons spend more and more time in the $R > R_0$ region. The magnetic field runaway electrons experience then tilts more towards the negative *z* direction on average, because of the helical configuration of the magnetic field lines. Since the parallel momentum is defined to be $p_\| = \mathbf{p} \cdot \mathbf{b}$, the change of $\mathbf{b}$ results in a change of $p_\|$. In the *z*-direction, the time average of momentum vanishes approximately, i.e. $\langle p_z \rangle = \langle p_{\|z} \rangle + \langle p_{\perp z} \rangle = 0$. Therefore, decrease of $\langle p_{\|z} \rangle$ corresponds to an increase of $\langle p_{\perp z} \rangle$.

The energy limit is reached at the saturation. The variation of the energy limit against the loop electric field with different magnetic field intensities are plotted in figure 6, which clearly shows that the energy limit depends on the strength of the background magnetic field. This is different from the conclusion by Martín-Solís *et al* using the gyro-center model [29]. Generally speaking, the energy limit given by gyro-center theory also depends on the strength of the background magnetic field, which can be incorporated in a gyro-kinetic code. However, according to [29], the radiation from gyro-motion is weak if the electric field is much stronger than the relativistic Dreicer field. Therefore, in gyro-center theory, when the loop electric field is strong enough, the dependence of energy limit on magnetic field is ignorable. The dashed line in figure 6 is calculated with electron density $n_e = 10^{19}\ m^{-3}$ and Coulomb logarithm $\ln\Lambda = 10$, which are typical tokamak parameters. According to the definition in [29], the normalized electric field *D* in this case is larger than 20, which corresponds to the

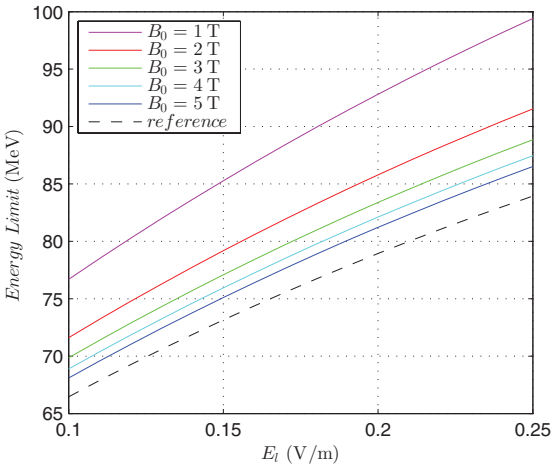

Figure 6. Plots of energy limit versus loop electric field E_l. The black dashed curve corresponds to the energy limit curve predicted by the gyro-center model [29], where collisional effect is ignorable. The solid curves correspond to energy limits with different magnetic field intensities. The loop electric field is set to be radially uniform in order to compare with the gyro-center model.

large electric field limit. Thus, the dashed line in figure 6 can be regarded as being independent of the background magnetic field. For comparison, other curves of energy limit in figure 6 show significant dependence on the magnetic field due to collisionless pitch-angle scattering. For the case of $B_0 = 1$ T, the real energy limit is about 20% higher, because more energy is transferred to the perpendicular direction through collisionless pitch-angle scattering. If the background magnetic field is extremely strong, the gyro-center approximation model will be valid, and the real energy limit curve will agree with the gyro-center result again.

In the present manuscript, we have focused on the effect of toroidal geometry of the background magnetic field, and the effect of field ripple has not been considered. Because the field ripple is small compared with the background field, its impact on the collisionless scattering should be weak in general. However, it is believed that a ripple field acts on the runaway dynamics through resonant effects to constrain the energy of runaway electrons. In this sense, it has a similar effect as the collisionless scattering. It is interesting to investigate the synergy effects when both collisionless scattering and magnetic ripple are considered.

In summary, long-term simulations using the newly developed VPA revealed that the full orbit dynamics of a runaway electron in the tokamak field geometry generate a pitch-angle scattering effect for runaway electrons. This effect is large enough to be detectable in experiments on major tokamaks. In a typical tokamak, this collisionless pitch-angle scattering is about one million times stronger than the collisional scattering and invalidates the gyro-center model for runaway electrons. As a consequence, the energy limit of runaway electrons is found to be larger than the prediction by a gyro-center model. In addition, the theoretical model developed in the present study shows that the runaway energy limit also depends heavily on the background magnetic field.

Acknowledgments

This research is supported by National Magnetic Confinement Fusion Energy Research Project (2015GB111003, 2014GB124005), National Natural Science Foundation of China (NSFC-11575185, 11575186, 11305171), JSPS-NRF-NSFC A3 Foresight Program (NSFC-11261140328), the CAS Program for Interdisciplinary Collaboration Team, and the GeoAlgorithmic Plasma Simulator (GAPS) Project.

References

[1] Dreicer H. 1959 *Phys. Rev.* **115** 238
[2] Yoshino R. *et al* 1997 *Plasma Phys. Control. Fusion* **39** 313
[3] Jaspers R. *et al* 1996 *Nucl. Fusion* **36** 367
[4] Helander P., Eriksson L.-G. and Andersson F. 2000 *Phys. Plasmas* **7** 4106
[5] Helander P., Eriksson L. and Andersson F. 2002 *Plasma Phys. Control. Fusion* **44** B247
[6] Fülöp T., Smith H. and Pokol G. 2009 *Phys. Plasmas* **16** 022502
[7] Gill R. *et al* 2000 *Nucl. Fusion* **40** 163
[8] Jaspers R. *et al* 1993 *Nucl. Fusion* **33** 1775
[9] Nygren R. *et al* 1997 *J. Nucl. Mater.* **241** 522
[10] Parks P., Rosenbluth M. and Putvinski S. 1999 *Phys. Plasmas* **6** 2523
[11] Rosenbluth M. and Putvinski S. 1997 *Nucl. Fusion* **37** 1355
[12] Yoshino R. and Tokuda S. 2000 *Nucl. Fusion* **40** 1293
[13] Tamai H. *et al* 2002 *Nucl. Fusion* **42** 290
[14] Lehnen M. *et al* 2008 *Phys. Rev. Lett.* **100** 255003
[15] Finken K. *et al* 2007 *Nucl. Fusion* **47** 91
[16] Fisch N.J. 1987 *Rev. Mod. Phys.* **59** 175
[17] Chen Z. *et al* 2006 *Phys. Lett.* A **351** 413
[18] Knoepfel H. and Spong D.A. 1979 *Nucl. Fusion* **19** 785
[19] Finken K. *et al* 1990 *Nucl. Fusion* **30** 859
[20] Wongrach K. *et al* 2014 *Nucl. Fusion* **54** 043011
[21] Jarvis O., Sadler G. and Thompson J. 1988 *Controlled Fusion and Plasma Heating Proc. 15th European Conf. (Dubrovnik, 1988)* vol 12B, part I
[22] Jarvis O., Sadler G. and Thompson J. 1988 *Nucl. Fusion* **28** 1981
[23] Gill R. 1993 *Nucl. Fusion* **33** 1613
[24] Chatelier M. *et al* 1989 *Controlled Fusion and Plasma Physics Proc. 16th European Conf. (Venice, 1989)* vol 13B, part I
[25] Bartels H.-W. 1994 *Fusion Eng. Des.* **23** 323
[26] Kawamura T., Obayashi H. and Miyahara A. 1989 *Fusion Eng. Des.* **9** 39
[27] Bolt H. *et al* 1987 *J. Nucl. Mater.* **151** 48
[28] Jaspers R. *et al* 2001 *Rev. Sci. Instrum.* **72** 466
[29] Martín-Solís J. *et al* 1998 *Phys. Plasmas* **5** 2370
[30] Martín-Solís J. *et al* 1999 *Phys. Plasmas* **6** 238
[31] Liu J. *et al* 2014 *Phys. Plasmas* **21** 064503
[32] Bakhtiari M. *et al* 2005 *Phys. Plasmas* **12** 102503
[33] Guan X., Qin H. and Fisch N.J. 2010 *Phys. Plasmas* **17** 092502
[34] Qin H., Guan X. and Fisch N.J. 2011 *Report* No. PPPL-4639 Princeton Plasma Physics Laboratory (PPPL), Princeton, NJ, USA
[35] Papp G. *et al* 2011 *Nucl. Fusion* **51** 043004
[36] Rax J., Fisch N. and Laurent L. 1993 *Plasma Phys. Control. Fusion* **35** B129
[37] Andersson F., Helander P. and Eriksson L.-G. 2001 *Phys. Plasmas* **8** 5221
[38] Littlejohn R.G. 1979 *J. Math. Phys.* **20** 2445
[39] Littlejohn R.G. 1981 *Phys. Fluids* **24** 1730

[40] Northrop T.G. 1963 *The Adiabatic Motion of Charged Particles* (New York: Interscience)
[41] Dalena S. *et al* 2012 *Phys. Rev.* E **86** 016402
[42] Dalena S. *et al* 2014 *Astrophys. J.* **783** 143
[43] Hastie R., Taylor J. and Haas F. 1967 *Ann. Phys.* **41** 302
[44] Hastie R., Hobbs G. and Taylor J. 1969 *Proc. 3rd Int. Conf. on Plasma Physics and Controlled Nuclear Fusion Research (Vienna, 1969)*
[45] Zhang R. *et al* 2015 *Phys. Plasmas* **22** 044501
[46] Jackson J.D. 1962 *Classical Electrodynamics* vol 3 (New York: Wiley)
[47] Qin H. and Guan X. 2008 *Phys. Rev. Lett.* **100** 035006
[48] He Y. *et al* 2015 *J. Comput. Phys.* **281** 135
[49] Qin H. *et al* 2013 *Phys. Plasmas* **20** 084503
[50] Xiao J. *et al* 2013 *Phys. Plasmas* **20** 102517
[51] Zhang R. *et al* 2014 *Phys. Plasmas* **21** 032504